Acta Cryst E CRYSTALLOGRAPHIC COMMUNICATIONS

ISSN 2056-9890

Crystal structure, supramolecular and Hirshfeld surface analysis of piperazine-1,4-diium bis(2,5-dibromobenzoate)

Veerappan Subha,[a]* Marimuthu Sathish[b]* and Thangavelu Balakrishnan[b]

[a]PG and Research Department of Physics, Government Arts College (Autonomous and affiliated to Bharathidasan University, Tiruchirappalli), Thanthonimalai, Karur-639 005, Tamil Nadu, India, and [b]Crystal Growth Laboratory, PG and Research Department of Physics, Thanthai Periyar Government Arts and Science College (Autonomous and affiliated to Bharathidasan, University, Tiruchirappalli), Tiruchirappalli-620 023, Tamil Nadu, India. *Correspondence e-mail: subha.prof@gmail.com, mksathisharasuss33@gmail.com

Received 27 May 2025
Accepted 4 August 2026

Edited by G. Ferrence, Illinois State University, USA

Keywords: crystal structure; proton transfer; piperazine-1,4-diium cation; 2,5-dibromobenzoate; Hirshfeld surface analysis.

CCDC reference: 2578701

Supporting information: this article has supporting information at journals.iucr.org/e

The title salt, $C_4H_{12}N_2^{2+}\cdot 2C_7H_3Br_2O_2^-$, crystallizes in the monoclinic space group $P2_1/c$ with $Z = 4$. The asymmetric unit comprises one-half of a piperazine-1,4-diium dication, located about an inversion center, and one 2,5-dibromobenzoate anion. In the dication, both nitrogen atoms of the piperazine ring are protonated, while the 2,5-dibromobenzoic acid is deprotonated at the carboxyl group. The proton is transferred from the acid to the piperazine molecule, resulting in the formation of the ionic salt. Charge neutrality is achieved by the presence of one dication for every two monobasic 2,5-dibromobenzoate anions. The piperazine ring adopts a chair conformation. The cations and anions are linked *via* N—H···O and N—H···Br hydrogen bonds, in which the carboxylate O atoms and Br atoms act as acceptors. These interactions (N—H···O/Br), together with additional C—H···Br contacts, contribute to the cohesion of the crystal structure. The resulting supramolecular architecture is analyzed in detail. Hirshfeld surface (HS) analysis, supported by two-dimensional fingerprint plots, indicates that H···O/O···H (47.5%) and H···Br/Br···H (34.0%) contacts are the major contributors for the cation, whereas H···Br/Br···H (31.6%) and H···O/O···H (21.4%) interactions dominate for the anion.

1. Chemical context

Piperazine is a six-membered heterocyclic aliphatic amine containing nitrogen atoms at the 1 and 4 positions, resulting in a symmetrical structure. These nitrogen atoms enable efficient hydrogen-bond formation, rendering piperazine a versatile organic base with high solubility in water and many organic solvents. Owing to these properties, piperazine exhibits significant biological relevance in pharmaceutical applications (Brito *et al.*, 2019; Shaquiquzzaman *et al.*, 2015) and is also widely utilized in industrial chemistry, making it a compound of considerable research interest. Furthermore, its ability to form stable supramolecular assemblies via non-covalent interactions has attracted attention in the fields of supramolecular chemistry and crystal engineering (Chen & Peng, 2008, 2011; Wang *et al.*, 2012; Priyanka *et al.*, 2022).

A search of the Cambridge Structural Database (CSD, Version 5.45, update of June 2024; Groom *et al.*, 2016; Ferrence *et al.*, 2023) reveals 69 structures of protonated piperazine-1,4-diium salts with substituted benzoate anions, including chloro-, amino-, nitro-, hydroxy-, and polycarboxy derivatives. The crystal structures and supramolecular features of related piperazine-1,4-diium salts with various counter-anions have been reported previously (Allu *et al.*, 2023;

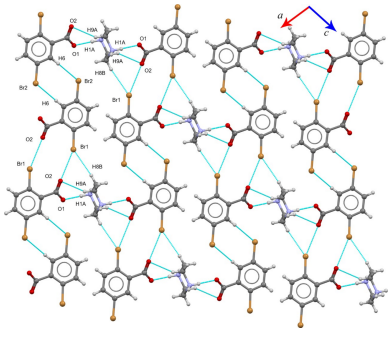

Roshini, & Jayalakshmi, 2023; Roy *et al.*, 2023; Sun *et al.*, 2023; Banik *et al.*, 2016).

As part of our ongoing studies on piperazine-based systems, including the hydrated 2:1 adduct of piperazine-1,4-diium-3,5-dinitro-2-oxidobenzoate with piperazine (Subha *et al.*, 2022*a*), and 4-(2-methoxyphenyl)piperazine-1-ium 3,5-dinitrosalicylate (Subha *et al.*, 2022*b*), we report herein the crystal structure of piperazine-1,4-diium bis(2,5-dibromobenzoate). The study includes detailed structural characterization, analysis of intermolecular interactions, and HS analysis (Spackman & Jayatilaka, 2009) to explore the supramolecular architecture.

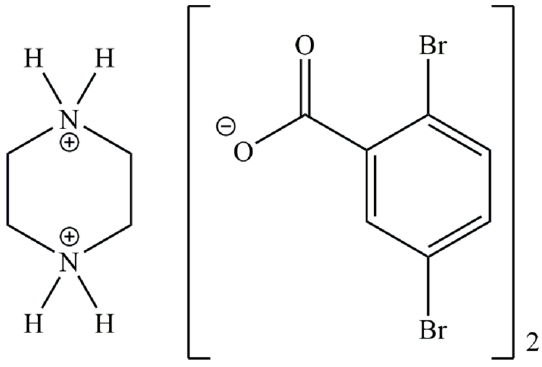

2. Structural commentary

The title salt (I) crystallizes in the monoclinic space group $P2_1/c$. The asymmetric unit comprises one-half of a piperazine-1,4-diium dication, located about an inversion center, and one 2,5-dibromobenzoate anion (Fig. 1). In the dication, both nitrogen atoms (N1 and its inversion-related equivalent) of the piperazine ring are protonated, while the 2,5-dibromobenzoic acid is deprotonated at the carboxyl group. Proton transfer from acid to piperazine molecule leads to the formation of the ionic salt. Charge neutrality is achieved by one dication for every two monobasic 2,5-dibromobenzoate anions in the crystal structure.

The piperazine ring adopts a chair conformation, with puckering parameters Q = 0.575 (3) Å, $\theta = 0°$, and $\varphi = 0°$. The geometric parameters, including bond lengths, bond angles, and torsion angles, for both dication and 2,5-dibromobenzoate anion are comparable to those reported for related structures.

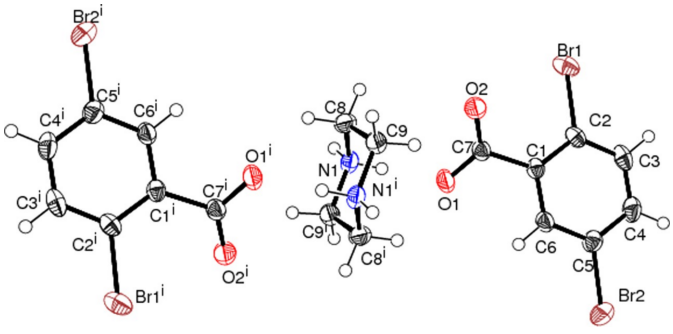

Figure 1
The molecular structure of the title molecular salt (I) showing the atom-labeling scheme. Displacement ellipsoids are drawn at the 50% probability level. Symmetry code: (i) $-x + 2, -y + 1, -z + 1$).

Table 1
Hydrogen-bond geometry (Å, °).

D—H···A	D—H	H···A	D···A	D—H···A
N1—H1A···O1	0.87 (2)	1.79 (2)	2.655 (3)	178 (4)
C9—H9A···O2	0.97	2.67	3.440 (4)	136
C6—H6···Br2^{i}	0.93	2.98	3.855 (3)	157
C8—H8A···Br2^{ii}	0.97	3.07	3.661 (3)	121
C8—H8B···Br1^{iii}	0.97	3.00	3.967 (3)	173
C9—H9A···Br1^{iv}	0.97	3.00	3.655 (3)	126
C9—H9B···Br2^{ii}	0.97	3.10	3.781 (3)	128
N1—H1B···O2^{v}	0.86 (2)	1.93 (2)	2.755 (3)	160 (3)
N1—H1B···Br1^{v}	0.86 (2)	3.06 (3)	3.598 (2)	123 (3)

Symmetry codes: (i) $-x+1, -y+1, -z+1$; (ii) $x+1, y, z$; (iii) $-x+2, -y+1, -z+2$; (iv) $x, -y+\frac{3}{2}, z-\frac{1}{2}$; (v) $-x+2, y-\frac{1}{2}, -z+\frac{3}{2}$.

In the crystal, the piperazine-1,4-diium cation and two 2,5-dibromobenzoate anions are connected via N1—H1A···O1 hydrogen bonding, complemented by additional C—H···Br interactions (Table 1), contributing to the cohesion of the crystal structure.

3. Supramolecular features

Both O atoms of the carboxylate group and Br atoms act as hydrogen-bond acceptors in a series of N—H···O, N—H···Br, and C—H···Br interactions within the crystal structure (Table 1). The carboxylate O atoms (O1 and O2) form hydrogen bonds with the protonated N atoms of the

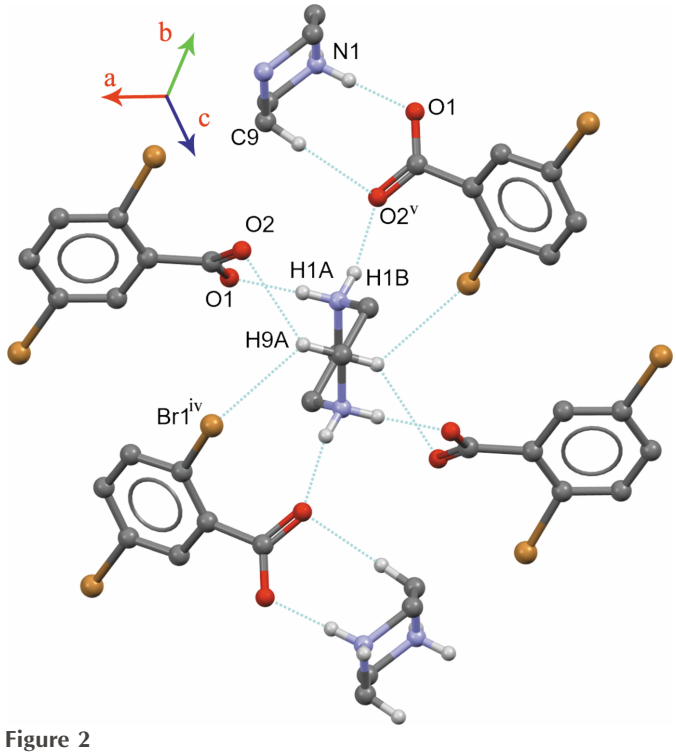

Figure 2
Part of the crystal structure of (I), showing the piperazine-1,4-diium cation linked to four neighboring anions *via* N1—H1A···O1, N1—H1B···O2, C9—H9A···O2, and C9—H9A···Br1 hydrogen bonds, forming a molecular double layer parallel to the *bc* plane. Symmetry codes as in Table 1.

piperazine-1,4-diium dication via N1—H1*A*···O1 and N1—H1*B*···O2^{v} [2.655 (3) Å and 2.755 (3) Å, respectively; symmetry code: (v) $-x+2, y-\frac{1}{2}, -z+\frac{3}{2}$]).

Each piperazine-1,4-diium cation is linked to four neighbouring anions through N—H···O, C—H···O/Br interactions [N1—H1*A*···O1, N1—H1*B*···O2^{v}, C9—H9*A*···O2 and C9—H9*A*···Br1^{iv}; symmetry code: (iv) $x, -y+\frac{3}{2}, z-\frac{1}{2}$], generating a molecular double layer parallel to the *bc* plane (Fig. 2).

Two neighbouring anions are further connected via a C6—H6···Br2^{i} hydrogen bond [symmetry code: (i) $-x+1, -y+1, -z+1$], forming a centrosymmetric $R_2^2(8)$ ring motif. In addition, adjacent motifs are linked through short C2═O2···Br1($-x+2, -y+1, -z+2$) contacts [3.3183 (2) Å], resulting in the formation of a molecular chain lying in the *ac* plane (Fig. 3).

The two-dimensional molecular layers are constructed through the combined N—H···O, C—H···O/Br interactions [N1—H1*A*···O1, C9—H9*A*···O2, C6—H6···Br, and C8—H8B···Br1] together with C2═O2···Br1 contacts, extending parallel to the *ac* plane (Fig. 4). These layers are further interconnected by additional N—H···O/Br, and C—H···O/Br interactions [C8—H8*A*···Br2^{ii}, C9—H9*A*···Br1^{iv}, C9—H9*B*···Br2^{ii}, N1—H1*B*···O2^{i}; N1—H1*B*···Br1^{v}], as well as a C—Br···π interaction involving the phenyl ring

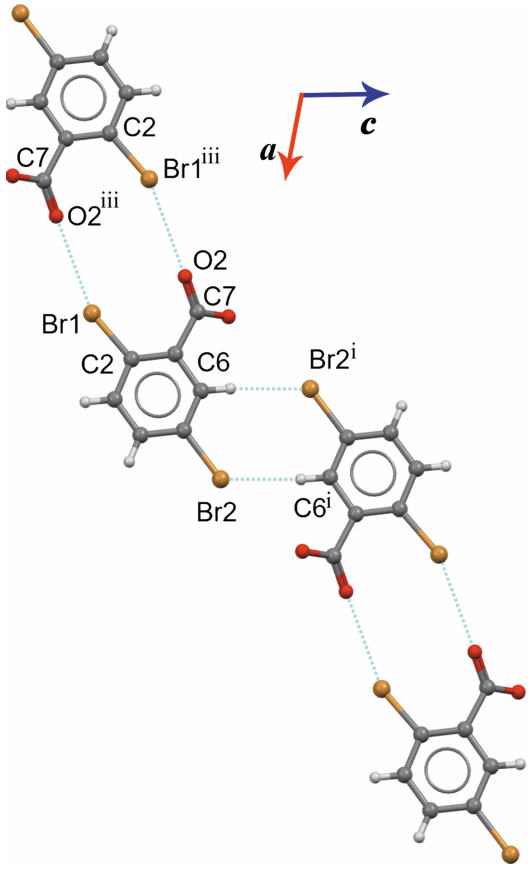

Figure 3
Part of the crystal structure of (I), showing a molecular chain formed *via* C6—H6···Br2 and C═O···Br interactions, viewed down the *b* axis. Symmetry codes as in Table 1.

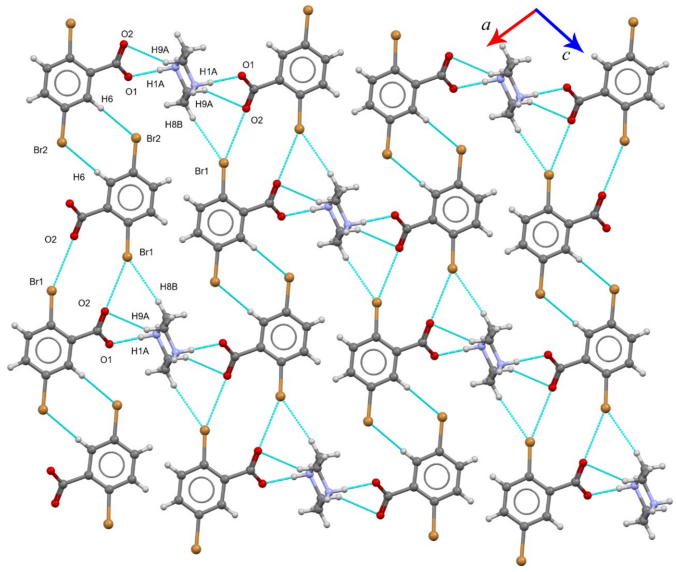

Figure 4
Part of the crystal structure of (I), showing a two-dimensional molecular layer formed *via* N1—H1*A*···O1, C9—H9*A*···O2, C6—H6···Br2, C8—H8*B*···Br1, and C═O···Br1 interactions, viewed down the *b* axis.

centroid [C5—Br2···*Cg*1($1-x, -\frac{1}{2}+y, \frac{1}{2}-z$) = 3.8107 (13) Å], leading to the formation of a three-dimensional supramolecular framework.

4. Hirshfeld surface analysis

Hirshfeld surfaces (HS) and two-dimensional fingerprint plots (2D-FP) were generated using *Crystal Explorer 17.5* (Turner *et al.*, 2017) for both the cation and the anion of the title salt. These analyses enable visualization and quantification of intermolecular interactions within the crystal packing (McKinnon *et al.*, 1998, 2004, 2007; Spackman & Jayatilaka, 2009; Spackman & McKinnon, 2002). The HS mapped over d_e (based on the distance from the surface to the nearest external atom) and d_i (distance from the nearest internal atom to the surface), facilitates identification of close contacts and their relative contributions. Variations in colors and intensities on the HS indicate short (red) and long (blue) contacts, highlight the significance of specific intermolecular interactions (Venkatesan *et al.*, 2015, 2016*a*,*b*). The decomposed 2D-FP plots provide a quantitative breakdown of individual contact contributions.

The HS mapped over d_{norm} in the range −0.75 to 1.1425 a.u. is shown (front and back) for both the dication and anion in Fig. 5*a*,*b*. Prominent bright-red spots correspond to strong hydrogen-bonding interactions, notably N1—H1*A*···O1 and N1—H1*B*···O2. Weaker red regions are associated with C—H···Br interactions, such as C6—H6···Br2 and C8—H8*B*···Br1. The C7═O2···Br1 contact is also visible as a weak red spot, suggesting a weak non-covalent interaction. The shape-index (SI) surfaces (Fig. 5*c*,*d*) do not display complementary red and blue triangular patterns over the aromatic rings, confirming the absence of π–π stacking interactions in the crystal structure.

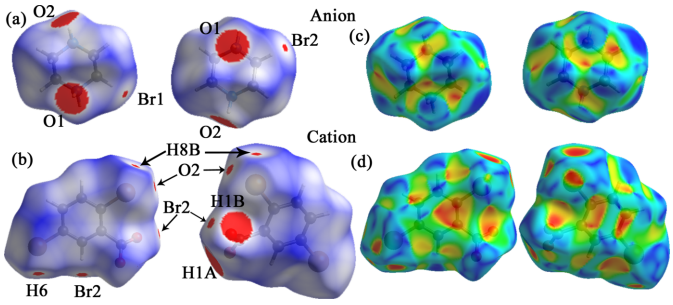

Figure 5
Hirshfeld surface of the cation and anion in the title salt shown in two orientations, mapped with (*a*) and (*b*) d_{norm} and (*c*) and (*d*) shape-index (SI).

The full and decomposed 2D-FP plots for the dication are shown in Fig. 6, with the corresponding percentage contributions summarized in Fig. 8. The dominant intermolecular contacts for the dication are H···O/O···H interactions, contributing 47.5% and appearing as a sharp spike at $d_e + d_i$ = 1.6 Å. The next major contribution arises from H···Br/Br···H contacts (34.0%), represented by a weak spike around $d_e + d_i$ = 3.0 Å. Minor contributions include H···C/C···H (10.7%) and H···H (7.8%) contacts.

In contrast, the anion (Fig. 7) is dominated by H···Br/Br···H interactions (31.6%), which appear as an asymmetric wing-like pattern at $d_e + d_i$ = 2.9 Å. The contribution of H···O/O···H contacts is 21.4%, and these still appear as sharp spikes near $d_e + d_i$ = 1.6 Å. This reduction is compensated by significant contributions from H···H (16.6%), H···C/C···H (15.4%), Br···O/O···Br (4.7%), and C···Br/Br···C (6.8%) interactions. These contacts arise from the involvement of Br atom in interactions such as C7═O2···Br1 and C5—Br2···*Cg*1, which are absent in the cation (where *Cg*1 is the centroid of the C1–C6 ring). The C···C contacts contribute only 3.1% in the anion and are negligible in the cation, confirming the absence of π–π interactions, in agreement with the shape-index analysis. Furthermore, the lack of significant features beyond $d_e + d_i$ = 2.4 Å suggests that H···H interactions play only a minor role in consolidating the crystal

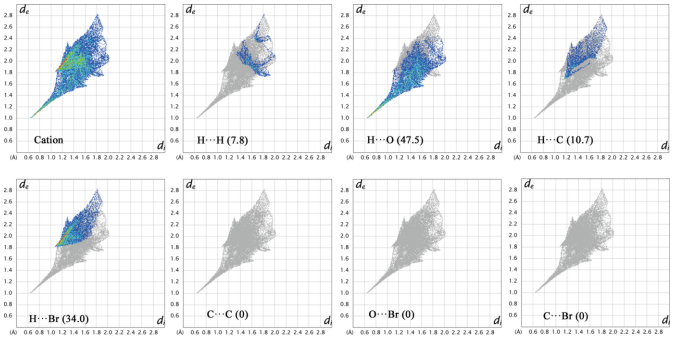

Figure 6
The full and decomposed two-dimensional fingerprint plots for the cation in the title salt (I), showing the relative contributions of the respective reciprocal contacts.

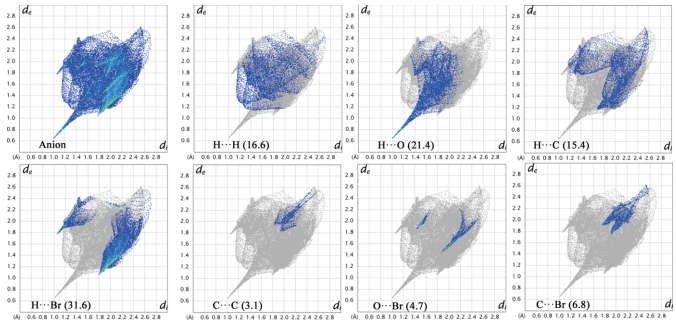

Figure 7
The full and decomposed two-dimensional fingerprint plots for the anion in the title salt (I), showing the relative contributions of the respective reciprocal contacts.

structure. The contributions of various interactions in the cation and anion are compared in Fig. 8.

5. Database survey

A search of the Cambridge Structural Database (CSD, Version 5.45, update of June 2024; Groom *et al.*, 2016) using Conquest (Bruno *et al.*, 2002) for piperazine-1,4-diium salts with substituted benzoic acids, including chloro-, amino-, nitro-, hydroxy-, and polycarboxy benzoic acids was performed. In particular, the crystal structures of piperazinediium bis(2/3/4-chlorobenzoate) (CSD refcodes ALOQIC, ALOQOI, ALOQUO; Chen & Peng 2011), piperazinediium bis(2-aminobenzoate) (ALORAV; Chen & Peng 2011); piperazinediium bis(4-aminobenzoate) (HEZTAI and HEZTAI01, Moulton *et al.*, 2007; Chen & Peng 2011) have been reported, and like the title compound, contain the piperazinediium ion.

6. Synthesis and crystallization

A 250 mL round-bottom flask was charged with piperazine (1 g, 11.6 mmol) and 2,5-dibromobenzoic acid (6.5 g, 23.2 mmol) in a 1:2 molar ratio. The mixture was dissolved in 50 mL of methanol at room temperature and stirred continuously for 6 h. The resulting homogeneous solution was filtered using Whatman filter paper and left undisturbed in a dust-free environment to evaporate slowly at room tempera-

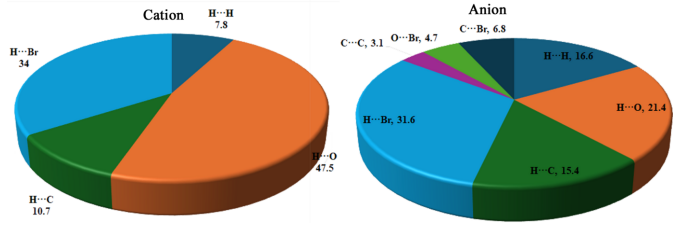

Figure 8
Pie charts showing the relative contributions of various intermolecular contacts to the Hirshfeld surfaces of the cation and anion in the title salt (I).

ture. After 10 days, red block-like crystals, with m.p. 458 K, suitable for single-crystal X-ray diffraction were obtained.

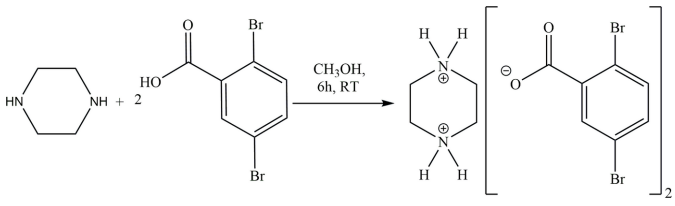

7. Refinement

Crystal data, data collection and structure refinement details are summarized in Table 2. The N-bound H atoms were located in a difference-Fourier map and refined with restrained N—H and H···H distances. C-bound H atoms were positioned geometrically (0.93–0.97 Å) and refined as riding with $U_{iso}(H) = 1.2U_{eq}(C)$.

Table 2
Experimental details.

Crystal data	
Chemical formula	$0.5C_4H_{12}N_2^{2+}\cdot C_7H_3Br_2O_2^-$
M_r	322.99
Crystal system, space group	Monoclinic, $P2_1/c$
Temperature (K)	298
a, b, c (Å)	11.7467 (5), 7.9755 (3), 11.3340 (4)
β (°)	101.052 (1)
V (Å^3)	1042.14 (7)
Z	4
Radiation type	Mo $K\alpha$
μ (mm^{-1})	7.75
Crystal size (mm)	0.23 × 0.20 × 0.15
Data collection	
Diffractometer	Bruker D8 VENTURE diffractometer equipped with PHOTON II detector
Absorption correction	Multi-scan (*SADABS*; Krause *et al.*, 2015)
T_{min}, T_{max}	0.462, 0.746
No. of measured, independent and observed [$I > 2\sigma(I)$] reflections	28846, 2565, 2133
R_{int}	0.056
$(\sin\theta/\lambda)_{max}$ (Å^{-1})	0.667
Refinement	
$R[F^2 > 2\sigma(F^2)]$, $wR(F^2)$, S	0.033, 0.073, 1.07
No. of reflections	2565
No. of parameters	135
No. of restraints	3
H-atom treatment	H atoms treated by a mixture of independent and constrained refinement
$\Delta\rho_{max}$, $\Delta\rho_{min}$ (e Å^{-3})	0.93, −0.75

Computer programs: *APEX4*, *SAINT* and *XPREP* (Bruker, 2021), *SHELXT* (Sheldrick, 2015*a*), *SHELXL2018/3* (Sheldrick, 2015*b*), *ORTEP-3 for Windows* (Farrugia, 2012), *PLATON* (Spek, 2020) and *Mercury* (Macrae *et al.*, 2020).

References

Allu, S., An, J.-H., Park, B. J. & Kim, W.-S. (2023). *Cryst. Growth Des.* **23**, 7231–7242.

Banik, M., Gopi, S. P., Ganguly, S. & Desiraju, G. R. (2016). *Cryst. Growth Des.* **16**, 5418–5428.

Brito, A. F., Moreira, L. K. S., Menegatti, R. & Costa, E. A. (2019). *Fundam. Clin. Pharmacol.* **33**, 13–24.

Bruker (2021). *APEX4 SAINT* and *XPREP*. Bruker AXS Inc., Madison, Wisconsin, USA.

Bruno, I. J., Cole, J. C., Edgington, P. R., Kessler, M., Macrae, C. F., McCabe, P., Pearson, J. & Taylor, R. (2002). *Acta Cryst.* B**58**, 389–397.

Chen, Z.-Y. & Peng, M.-X. (2008). *Chin. J. Chem.* **26**, 1555–1560.

Chen, Z.-Y. & Peng, M.-X. (2011). *J. Chem. Crystallogr.* **41**, 137–142.

Farrugia, L. J. (2012). *J. Appl. Cryst.* **45**, 849–854.

Ferrence, G. M., Tovee, C. A., Holgate, S. J. W., Johnson, N. T., Lightfoot, M. P., Nowakowska-Orzechowska, K. L. & Ward, S. C. (2023). *IUCrJ* **10**, 6–15.

Groom, C. R., Bruno, I. J., Lightfoot, M. P. & Ward, S. C. (2016). *Acta Cryst.* B**72**, 171–179.

Krause, L., Herbst-Irmer, R., Sheldrick, G. M. & Stalke, D. (2015). *J. Appl. Cryst.* **48**, 3–10.

McKinnon, J. J., Jayatilaka, D. & Spackman, M. A. (2007). *Chem. Commun.* pp. 3814–3816.

McKinnon, J. J., Mitchell, A. S. & Spackman, M. A. (1998). *Chem. Eur. J.* **4**, 2136–2141.

McKinnon, J. J., Spackman, M. A. & Mitchell, A. S. (2004). *Acta Cryst.* B**60**, 627–668.

Macrae, C. F., Sovago, I., Cottrell, S. J., Galek, P. T. A., McCabe, P., Pidcock, E., Platings, M., Shields, G. P., Stevens, J. S., Towler, M. & Wood, P. A. (2020). *J. Appl. Cryst.* **53**, 226–235.

Moulton, B., Luisi, B. S., Fonari, M. S., Basok, S. S., Ganin, E. V. & Kravtsov, V. C. (2007). *New J. Chem.* **31**, 561–568.

Priyanka, P., Jayanna, B. K., Divakara, T. R., Suresha, G. P., Vinaya, Basavaraju, Y. B., Yathirajan, H. S., Parkin, S. R. & Chęcińska, L. (2022). *Crystals* **12**, 1807.

Roshini, S. R. A. & Jayalakshmi, D. (2023). *Opt. Mater.* **146**, 114577.

Roy, P., Chakraborty, S., Pandey, N., Kumari, N., Chougule, S., Chatterjee, A., Chatterjee, K., Mandal, P., Gorain, B., Dhotre, A. V., Bansal, A. K. & Ghosh, A. (2023). *Mol. Pharm.* **20**, 5226–5239.

Shaquiquzzaman, M., Verma, G., Marella, A., Akhter, M., Akhtar, W., Khan, M. F., Tasneem, S. & Alam, M. M. (2015). *Eur. J. Med. Chem.* **102**, 487–529.

Sheldrick, G. M. (2015*a*). *Acta Cryst.* A**71**, 3–8.

Sheldrick, G. M. (2015*b*). *Acta Cryst.* C**71**, 3–8.

Spackman, M. A. & Jayatilaka, D. (2009). *CrystEngComm* **11**, 19–32.

Spackman, M. A. & McKinnon, J. J. (2002). *CrystEngComm* **4**, 378–392.

Spek, A. L. (2020). *Acta Cryst.* E**76**, 1–11.

Subha, V., Seethalakshmi, T., Balakrishnan, T., Percino, M. J. & Venkatesan, P. (2022*a*). *Acta Cryst.* E**78**, 198–202.

Subha, V., Seethalakshmi, T., Balakrishnan, T., Percino, M. J. & Venkatesan, P. (2022*b*). *Acta Cryst.* E**78**, 774–778.

Sun, R., Braun, D. E., Casali, L., Braga, D. & Grepioni, F. (2023). *Cryst. Growth Des.* **23**, 1874–1887.

Turner, M., McKinnon, J., Wolff, S., Grimwood, D., Spackman, P., Jayatilaka, D. & Spackman, M. (2017). *CrystalExplorer17.5*. University of Western Australia.

Venkatesan, P., Rajakannan, V., Venkataramanan, N. S., Ilangovan, A., Sundius, T. & Thamotharan, S. (2016*a*). *J. Mol. Struct.* **1119**, 259–268.

Venkatesan, P., Thamotharan, S., Ilangovan, A., Liang, H. & Sundius, T. (2016*b*). *Spectrochim. Acta A Mol. Biomol. Spectrosc.* **153**, 625–636.

Venkatesan, P., Thamotharan, S., Kumar, R. G. & Ilangovan, A. (2015). *CrystEngComm* **17**, 904–915.

Wang, L., Zhao, L., Xu, L., Chen, R. & Yang, Y. (2012). *CrystEngComm* **14**, 6998–7008.

supporting information

Acta Cryst. (2026). E**82**, 1057-1061 [https://doi.org/10.1107/S205698902600798X]

Crystal structure, supramolecular and Hirshfeld surface analysis of piperazine-1,4-diium bis(2,5-dibromobenzoate)

Veerappan Subha, Marimuthu Sathish and Thangavelu Balakrishnan

Computing details

Piperazine-1,4-diium bis (2,5-dibromobenzoate)

Crystal data

$0.5C_4H_{12}N_2^{2+}\cdot C_7H_3Br_2O_2^-$
M_r = 322.99
Monoclinic, $P2_1/c$
a = 11.7467 (5) Å
b = 7.9755 (3) Å
c = 11.3340 (4) Å
β = 101.052 (1)°
V = 1042.14 (7) Å^3
Z = 4
$F(000)$ = 624
D_x = 2.059 Mg m^{-3}
Mo $K\alpha$ radiation, λ = 0.71073 Å
Cell parameters from 9898 reflections
θ = 3.1–27.9°
μ = 7.75 mm^{-1}
T = 298 K
Block, colourless
0.23 × 0.20 × 0.15 mm

Data collection

Bruker D8 VENTURE diffractometer equipped with PHOTON II detector
Radiation source: fine-focus sealed tube
ω and phi scans
Absorption correction: multi-scan (SADABS; Krause *et al.*, 2015)
T_{min} = 0.462, T_{max} = 0.746
28846 measured reflections
2565 independent reflections
2133 reflections with $I > 2\sigma(I)$
R_{int} = 0.056
θ_{max} = 28.3°, θ_{min} = 3.4°
h = −15→15
k = −10→10
l = −15→15

Refinement

Refinement on F^2
Least-squares matrix: full
$R[F^2 > 2\sigma(F^2)]$ = 0.033
$wR(F^2)$ = 0.073
S = 1.07
2565 reflections
135 parameters
3 restraints
Hydrogen site location: mixed
H atoms treated by a mixture of independent and constrained refinement
$w = 1/[\sigma^2(F_o^2) + (0.0208P)^2 + 1.9785P]$ where $P = (F_o^2 + 2F_c^2)/3$
$(\Delta/\sigma)_{max}$ = 0.001
$\Delta\rho_{max}$ = 0.93 e Å^{-3}
$\Delta\rho_{min}$ = −0.75 e Å^{-3}

Special details

Geometry. All esds (except the esd in the dihedral angle between two l.s. planes) are estimated using the full covariance matrix. The cell esds are taken into account individually in the estimation of esds in distances, angles and torsion angles; correlations between esds in cell parameters are only used when they are defined by crystal symmetry. An approximate (isotropic) treatment of cell esds is used for estimating esds involving l.s. planes.

Fractional atomic coordinates and isotropic or equivalent isotropic displacement parameters (Å²)

	x	*y*	*z*	U_{iso}*/U_{eq}
C1	0.7131 (2)	0.5605 (3)	0.7922 (2)	0.0246 (5)
C2	0.6993 (3)	0.5879 (4)	0.9100 (2)	0.0275 (6)
C3	0.5922 (3)	0.6344 (4)	0.9357 (3)	0.0359 (7)
H3	0.584948	0.651873	1.015030	0.043*
C4	0.4973 (3)	0.6545 (4)	0.8449 (3)	0.0365 (7)
H4	0.426181	0.687138	0.861885	0.044*
C5	0.5096 (2)	0.6255 (4)	0.7280 (3)	0.0306 (6)
C6	0.6150 (2)	0.5787 (4)	0.7012 (3)	0.0275 (6)
H6	0.620851	0.559147	0.621684	0.033*
C7	0.8252 (2)	0.5091 (4)	0.7527 (2)	0.0263 (6)
C8	1.0922 (3)	0.4660 (4)	0.6006 (3)	0.0312 (6)
H8A	1.155531	0.435851	0.561002	0.037*
H8B	1.120077	0.459490	0.686723	0.037*
C9	1.0533 (3)	0.6428 (4)	0.5665 (3)	0.0308 (6)
H9A	0.994383	0.676443	0.611181	0.037*
H9B	1.118506	0.718859	0.587074	0.037*
N1	0.9947 (2)	0.3469 (3)	0.5648 (2)	0.0278 (5)
O1	0.81248 (19)	0.4115 (3)	0.6644 (2)	0.0428 (6)
O2	0.91953 (18)	0.5667 (3)	0.8059 (2)	0.0386 (5)
Br1	0.82116 (3)	0.54666 (5)	1.04365 (3)	0.04140 (11)
Br2	0.37973 (3)	0.64277 (5)	0.60002 (3)	0.04320 (11)
H1A	0.936 (2)	0.367 (4)	0.599 (3)	0.049 (11)*
H1B	1.021 (3)	0.249 (3)	0.588 (3)	0.044 (10)*

Atomic displacement parameters (Å²)

	U^{11}	U^{22}	U^{33}	U^{12}	U^{13}	U^{23}
C1	0.0252 (13)	0.0234 (13)	0.0270 (13)	−0.0029 (10)	0.0095 (10)	−0.0019 (11)
C2	0.0349 (15)	0.0261 (14)	0.0226 (12)	−0.0049 (11)	0.0081 (11)	−0.0014 (11)
C3	0.0446 (18)	0.0386 (18)	0.0296 (15)	−0.0032 (14)	0.0198 (13)	−0.0064 (13)
C4	0.0317 (15)	0.0417 (18)	0.0409 (17)	0.0007 (13)	0.0193 (13)	−0.0041 (14)
C5	0.0256 (14)	0.0322 (16)	0.0350 (15)	−0.0008 (12)	0.0082 (12)	−0.0010 (13)
C6	0.0286 (14)	0.0318 (15)	0.0240 (13)	−0.0006 (11)	0.0097 (11)	−0.0026 (11)
C7	0.0280 (14)	0.0286 (14)	0.0236 (12)	0.0003 (11)	0.0081 (11)	0.0003 (11)
C8	0.0263 (14)	0.0376 (17)	0.0284 (14)	0.0014 (12)	0.0018 (11)	0.0021 (13)
C9	0.0307 (14)	0.0325 (15)	0.0298 (14)	0.0005 (12)	0.0075 (11)	−0.0036 (12)
N1	0.0275 (12)	0.0295 (13)	0.0290 (12)	0.0058 (10)	0.0117 (10)	0.0042 (10)
O1	0.0286 (11)	0.0612 (15)	0.0404 (12)	−0.0026 (10)	0.0111 (9)	−0.0251 (12)
O2	0.0274 (11)	0.0489 (14)	0.0395 (12)	−0.0045 (10)	0.0063 (9)	−0.0148 (11)
Br1	0.0485 (2)	0.0501 (2)	0.02394 (15)	−0.00516 (15)	0.00278 (12)	0.00032 (14)
Br2	0.02605 (16)	0.0556 (2)	0.0469 (2)	0.00428 (14)	0.00450 (13)	−0.00056 (16)

Geometric parameters (Å, º)

C1—C2	1.392 (4)	C7—O2	1.243 (4)
C1—C6	1.399 (4)	C7—O1	1.254 (4)
C1—C7	1.526 (4)	C8—N1	1.484 (4)
C2—C3	1.395 (4)	C8—C9	1.510 (4)
C2—Br1	1.903 (3)	C8—H8A	0.9700
C3—C4	1.374 (5)	C8—H8B	0.9700
C3—H3	0.9300	C9—N1^{i}	1.488 (4)
C4—C5	1.379 (4)	C9—H9A	0.9700
C4—H4	0.9300	C9—H9B	0.9700
C5—C6	1.382 (4)	N1—H1A	0.870 (18)
C5—Br2	1.897 (3)	N1—H1B	0.864 (17)
C6—H6	0.9300		
C2—C1—C6	117.4 (3)	O1—C7—C1	115.0 (2)
C2—C1—C7	126.1 (3)	N1—C8—C9	110.4 (2)
C6—C1—C7	116.5 (2)	N1—C8—H8A	109.6
C1—C2—C3	121.2 (3)	C9—C8—H8A	109.6
C1—C2—Br1	121.9 (2)	N1—C8—H8B	109.6
C3—C2—Br1	116.8 (2)	C9—C8—H8B	109.6
C4—C3—C2	120.6 (3)	H8A—C8—H8B	108.1
C4—C3—H3	119.7	N1^{i}—C9—C8	110.2 (2)
C2—C3—H3	119.7	N1^{i}—C9—H9A	109.6
C3—C4—C5	118.7 (3)	C8—C9—H9A	109.6
C3—C4—H4	120.6	N1^{i}—C9—H9B	109.6
C5—C4—H4	120.6	C8—C9—H9B	109.6
C4—C5—C6	121.3 (3)	H9A—C9—H9B	108.1
C4—C5—Br2	120.3 (2)	C8—N1—C9^{i}	111.2 (2)
C6—C5—Br2	118.3 (2)	C8—N1—H1A	113 (3)
C5—C6—C1	120.8 (3)	C9^{i}—N1—H1A	105 (3)
C5—C6—H6	119.6	C8—N1—H1B	107 (3)
C1—C6—H6	119.6	C9^{i}—N1—H1B	113 (3)
O2—C7—O1	125.1 (3)	H1A—N1—H1B	107 (2)
O2—C7—C1	119.8 (3)		
C6—C1—C2—C3	−1.0 (4)	Br2—C5—C6—C1	−178.6 (2)
C7—C1—C2—C3	−179.9 (3)	C2—C1—C6—C5	1.3 (4)
C6—C1—C2—Br1	173.8 (2)	C7—C1—C6—C5	−179.8 (3)
C7—C1—C2—Br1	−5.0 (4)	C2—C1—C7—O2	−37.1 (4)
C1—C2—C3—C4	−0.1 (5)	C6—C1—C7—O2	144.1 (3)
Br1—C2—C3—C4	−175.2 (3)	C2—C1—C7—O1	144.3 (3)
C2—C3—C4—C5	1.0 (5)	C6—C1—C7—O1	−34.5 (4)
C3—C4—C5—C6	−0.7 (5)	N1—C8—C9—N1^{i}	−56.7 (3)
C3—C4—C5—Br2	177.4 (2)	C9—C8—N1—C9^{i}	57.4 (3)
C4—C5—C6—C1	−0.4 (5)		

Symmetry code: (i) −*x*+2, −*y*+1, −*z*+1.

Hydrogen-bond geometry (Å, º)

D—H···*A*	*D*—H	H···*A*	*D*···*A*	*D*—H···*A*
N1—H1*A*···O1	0.87 (2)	1.79 (2)	2.655 (3)	178 (4)
C9—H9*A*···O2	0.97	2.67	3.440 (4)	136
C6—H6···Br2^{ii}	0.93	2.98	3.855 (3)	157
C8—H8*A*···Br2^{iii}	0.97	3.07	3.661 (3)	121
C8—H8*B*···Br1^{iv}	0.97	3.00	3.967 (3)	173
C9—H9*A*···Br1^{v}	0.97	3.00	3.655 (3)	126
C9—H9*B*···Br2^{iii}	0.97	3.10	3.781 (3)	128
N1—H1*B*···O2^{vi}	0.86 (2)	1.93 (2)	2.755 (3)	160 (3)
N1—H1*B*···Br1^{vi}	0.86 (2)	3.06 (3)	3.598 (2)	123 (3)

Symmetry codes: (ii) −*x*+1, −*y*+1, −*z*+1; (iii) *x*+1, *y*, *z*; (iv) −*x*+2, −*y*+1, −*z*+2; (v) *x*, −*y*+3/2, *z*−1/2; (vi) −*x*+2, *y*−1/2, −*z*+3/2.